RSC Advances




ROYAL SOCIETY OF CHEMISTRY

www.rsc.org/advances

Journal Name

ARTICLE

# High performance sponge $MnO_2$ nanotube monoliths

Guangwu Yang,*[a,b] Bing He,[a] Fuzhen Zhao,[a] Wenyue Guo,*[a,b] Qingzhong Xue[a,b] and Hulin Li[c]

Received 00th January 20xx,
Accepted 00th January 20xx

DOI: 10.1039/x0xx00000x

www.rsc.org/

Self-supported sponge $MnO_2$ nanotube monoliths (SMM) are synthesized via a hydrothermal method using commercial polyurethane foam as a sacrificial template. The SMM with its three-dimensional interconnected foam structure, macroporous channels, and mesoporous tube structure endow this novel material with a diversity of porous architectures and great promise for various applications as sorbents, catalysts, ion exchanges, and energy storage. As a proof of application, we have demonstrated that SMM-based supercapacitor exhibits excellent capacitance behavior and rate capability.

## Introduction

Porous materials are of scientific and technological interest because of their ability to interact with atoms, ions and molecules not only at their surfaces, but throughout the bulk of the material. The understanding, design, and manipulation of porous materials are playing increasingly important roles in a wide range of potential applications involving catalysis, sorption, gas sensing, ion exchange, optics, and photovoltaics.[1-4]

According to IUPAC notation, porous materials are classified into three categories by their pore size, namely microporous, mesoporous, and macroporous with pore sizes less than 2 nm, between 2 and 50 nm, and larger than 50 nm, respectively.[5] Macropores facilitate bulk diffusion and viscous flow, such as the transport of water, ions and proteins, while mesopores and micropores dominate surface diffusion and activated transport. Therefore, the distribution of pore sizes directly relates to their ability to perform the desired function in a particular application. However, in many cases, unimodal micro-, meso-, or macroporous materials cannot satisfy the porous high-performance applications. The need to create hierarchical porous materials (HPMs) simultaneously with bimodal or multimodal pore-size distributions has steadily increased over recent years, because it can lead to superior application properties. For example, HPMs combining macropores and mesopores make it easy for the fast transportation of ions, water, or even large molecules because they can effectively access the mesopores and/or micropores interconnected by the macropore system.[6-11] These advantages make it one of the best candidates for high performance energy storage applications such as supercapacitors, lithium-ion batteries, and fuel cells.[12] A common strategy to synthesis HPMs is to use two or more templates of different sizes. Although hierarchical porous silicas and carbons have been reported,[13, 14] there are very few reports in the literatures on hierarchical porous metal oxides, such as $MnO_2$, which is the most thoroughly investigated transition metal oxide for pseudocapacitors due to its high theoretical specific capacitance (1370 F $g^{-1}$), low cost, and environmental friendliness.[15-17] In addition, how to realize the mass production of HPMs through a practical and economic approach is still a challenge.

Here, for the first time, we report a novel structured HPM, self-supported sponge $MnO_2$ nanotube monoliths (SMM), which allows for any arbitrary shape of monolithic $MnO_2$ with dimensional scalability, mass-production capability, and pore structure parameter controllability. The SMM can be simply prepared via a one-step hydrothermal procedure using polyurethane (PU) foam as a sacrificial template. With large specific surface area, three-dimensional (3D) interconnected pathways, and well-defined multimodal pore structure, the SMM holds great promise for applications in various energy storage devices, such as supercapacitors. To the best of our knowledge, this monolithic $MnO_2$ with hierarchical porous architecture has not yet been reported.

## Experimental

### Fabrication of SMM

SMM is synthesized via a simple one-step hydrothermal approach. A piece of PU foam (pore sizes 300~500 μm) is successively cleaned by deionized water and ethanol in an ultrasound bath for 5 min. After drying completely, the PU foam is transferred to a 100-mL autoclave containing 1.5 g $KMnO_4$, 0.275 g $MnSO_4 \cdot H_2O$, and 80 mL

[a] College of Science, China University of Petroleum, Qingdao, 266580, P. R. China. E-mail: yanggw@upc.edu.cn.
[b] Key Laboratory of New Energy Physics & Materials Science in Universities of Shandong, China University of Petroleum, Qingdao, 266580, P. R. China.
[c] College of Chemistry and Chemical Engineering, Lanzhou University, Lanzhou 730000, P.R. China.

deionized water and hydrothermal reacted at 240 °C for 24 h. The obtained material is washed with deionized water and ethanol several times, and then dried at 60 °C for 12 h in air. Calcination is carried out in a muffle furnace at a ramp of 1 °C/min from room temperature to 500 °C, and kept for 3 h to optimize the crystal structure of $MnO_2$ and further remove the template residue.

**Material characterizations**

X-Ray Diffraction (XRD) patterns are collected using a Rigaku D/MAX 2700 diffractometer (Japan) with Cu-Kα radiation (k = 1.5418 Å) operating at 40.0 kV, 60.0 mA. Surface morphology of the samples is examined by Field Emission Scanning Electron Microscopy (FESEM, JEOL JSM-S4800) and Transmission Electron Microscopy (TEM, JEM-2100). Specific surface area and pore size distribution are analyzed via Brunauer–Emmett–Teller (BET) method and Barrett–Joyner–Halenda (BJH) method at -196 °C by using a TriStar 3000 equipment.

**Electrochemical measurements**

The electrochemical performance of SMM is tested using a three-electrode cell configuration containing 1 M $Na_2SO_4$ aqueous solution as the electrolyte. An Ag/AgCl electrode is used as the reference and a platinum sheet electrode is employed as the counter electrode. The SMM-based electrode is fabricated by mixing on piece of SMM (80 wt%), acetylene black (15 wt%) and polytetrauoroethylene (5 wt%). A slurry of acetylene black and polytetrauoroethylene is pre-prepared using N-methyl-2-pyrrolidone as a solvent, which is subsequently brushed onto the SMM and frequently remove the air bubbles with a glass rod during the infusion of sol solution. After drying, the coated SMM is clamped using a folded nickel foam current collector without destroying the whole structure of SMM. For comparision, another piece of SMM is grinded in an agate mortar into $MnO_2$ powders, which is used to prepare $MnO_2$ powder-based electrode. Cyclic voltammetry (CV), galvanostatic charge–discharge and electrochemical impedance spectroscopy (EIS) measurements are all performed on a CHI760d Electrochemical Workstation at room temperature.

## Results and discussion

**Structure and morphology characterization**

The main paragraph text follows directly on here. PU foam is widely used in our daily life, such as cleaning tools. It is made up of molecular chains bounded together by carbamate links, which make it highly porous and hydrophilous. PU foam can be easily tailored and employed as a macrostructure sacrificial template for the synthesis of monolithic materials with various desired geometric shapes (Fig. 1).

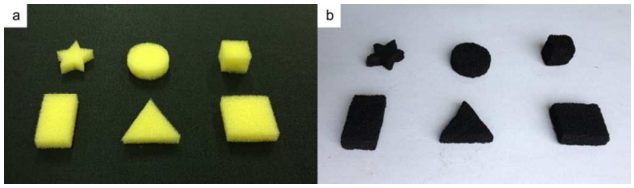


**Fig. 1** Photograph of the commercial PU foams cut into various geometric shapes (a), and as-synthesized SMM templated by PU foam (b).

The FESEM image of pure PU foam shows clearly 3D interconnecting networks with much more uniform macropores of 300~500 μm (Fig. 2a). After hydrothermal reaction, $MnO_2$ nanotubes are uniformly grown and coated onto the foam skeleton, forming a monolithic $MnO_2$ nanotube sponge templated perfectly by PU foam (Figure 2b). It is noticed that the backbone of PU foam is free of junctions, which promotes the continuous coating of $MnO_2$ nanotubes to form integrated conducting pathways. Especially, the removal of PU foam creates interconnected macroporous channels in the whole structure, which are predicted to promote the diffusion of electrolytes. The $MnO_2$ nanotubes with a diameter range of 10~50 nm are long and tangled together with each other (Fig. 2c and 2d), which essentially provide this relatively light monolithic material with certain degree of mechanical strength.

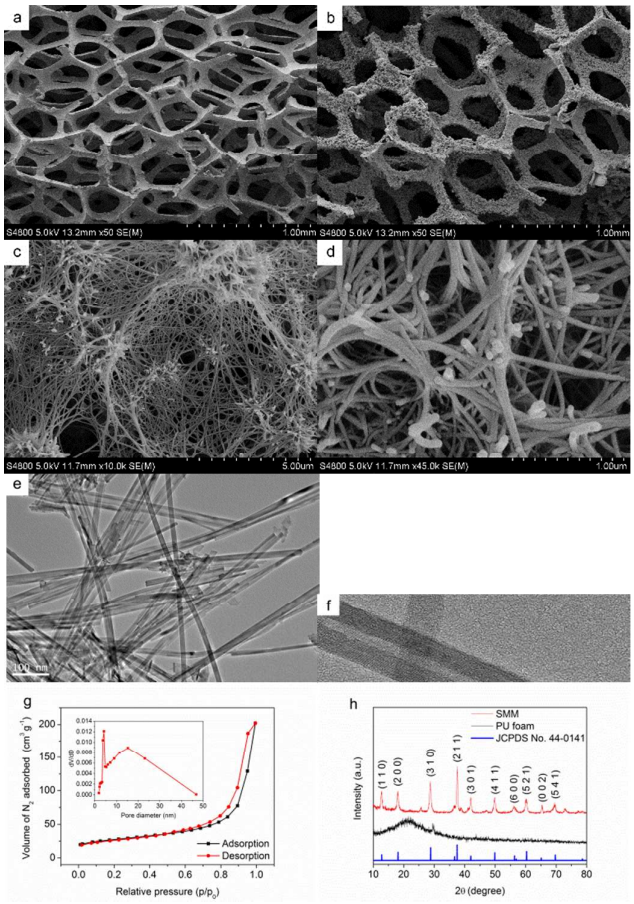


**Fig. 2** FESEM images of PU foam (a), and SMM at different magnification (b-d); TEM images of $MnO_2$ nanotubes at different magnification (e-f); Nitrogen adsorption–desorption isotherms of SMM (Insets: the corresponding BJH pore size distribution curves calculated from desorption branch) (g); and XRD patterns of the reference $MnO_2$ powders, PU foam, and SMM (h).

From TEM image of Fig. 2e, one can identify the hollow structure of $MnO_2$ nanotubes. Closed examination of Fig. 2f shows that the $MnO_2$ nanotubes are uniform with a through pore size of about 4.5 nm. Lattice fringes with interplanar spacing of 0.31 nm can be well found, which matches well with (3 1 0) planes of tetragonal $MnO_2$. The hollow mesoporous structure is predicted to increase more active sites.[18]

The porosity of the SMM is studied by nitrogen sorption. The nitrogen adsorption–desorption isotherm in Fig. 2g shows a type IV hysteresis loop at p/p0 = 0.5–1.0, suggesting a hybrid porous structure.[19] Significant nitrogen uptake at the high relative pressure region (P/P0 > 0.9) is associated with multilayer adsorption on a macroporous solid. The pore size distribution is clearly reflected by BJH curve, it can be seen that there are two peaks, a sharp one at 4.2 nm and a broad one at 5–45 nm, corresponding to the inner diameter of $MnO_2$ nanotubes and porous surface structure of SMM. The BET surface area and BJH pore volumes of the SMM are calculated from the isotherm curves to be 92 $m^2 g^{-1}$ and 0.31 $cm^3 g^{-1}$, respectively.

Fig. 2h illustrates the XRD patterns of PU foam and the SMM after heat treatment. All the diffraction peaks of $MnO_2$ located at 2θ values of 10–80° agree well with the tetragonal α-$MnO_2$ (JCPDS No. 44-0141). Compared with the patterns of PU foam, no characteristic peaks can be observed, indicating that the PU foam has been completely removed.

**Electrochemical properties**

The SMM with its 3D interconnected foam structure, macroporous channels, and mesoporous tube structure provides outstanding performance for the intercalation/deintercalation of electrolyte cations into electrode materials, which is expected to fabricate high-performance supercapacitors. To evaluate the electrochemical performance of SMM, CV, galvanostatic charge–discharge, and EIS are performed in a three-electrode configuration.

Fig. 3a shows the CV curves of SMM-based electrode at various scan rates. The shape of the voltammograms shows a rectangular image corresponding to a typical capacitive behavior for $MnO_2$, indicating an ideal electrical double layer capacitance behavior and fast charging/discharging process characteristics.[20, 21] The area enclosed by the CV curves and the current increase with the increase of scan rates. Even at a high scan rate of 0.1 V $s^{-1}$, the shapes of the curves remain undistorted, implying a low contact resistance of the supercapacitor.

Galvanostatic charge–discharge measurements are performed at different current densities as shown in Fig. 3b. The specific capacitance of the SMM-based electrode depending on the mass of the active material values are calculated to be 325, 305, 280, and 252 F $g^{-1}$ corresponding to the charge–discharge current densities of 1, 2 , 4, and 8 A $g^{-1}$, respectively. The linear voltage versus time profiles and the quick I–V response suggest that the SMM are good electrode materials for supercapacitors. SMM is grinded into $MnO_2$ powders to destroy the hierarchical porous structure and 3D interconnecting network, and tested under the same conditions. It is observed that the $MnO_2$ powders exhibit narrower CV curves and lower capacitance (Fig. 3c and 3d).

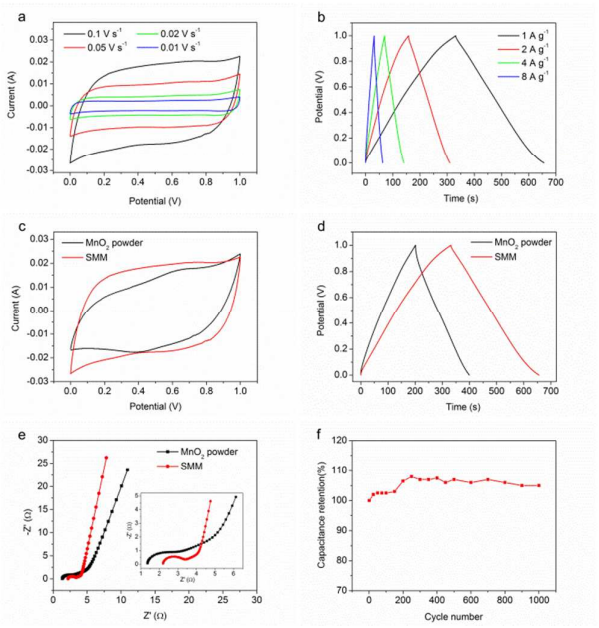


**Fig. 3** Electrochemical properties of SMM-based electrode: CV curves at different scan rates (a); galvanostatic charge–discharge at different discharge current densities (b); Compared electrochemical properties of SMM-based electrode and $MnO_2$ powders: CV curves at a scan rate of 0.1 V $s^{-1}$ (c), galvanostatic charge–discharge at a discharge current density of 1 A $g^{-1}$ (d), Nyquist plots at the open circuit potential (e); and cycle life data of SMM-based electrode at a discharge current density of 4 A $g^{-1}$ (f).

Therefore, the remarkable performance of SMM can be attributed to its unique architecture. Firstly, the 3D interconnected foam structure endows continuous conducting pathways, facilitating the transport of electrons. Secondly, the macroporous channels in the whole structure serving as the "ion-buffering reservoirs", minimize the diffusion distance to the interior surface, accelerating the kinetic process of the ion diffusion in the electrode.[22, 23] And thirdly, the mesoporous tube structure provides abundant surfaces for charge–transfer reactions, ensuring a high utilization of active materials. This is further proved by EIS results presented in Fig 3e. The semicircle at high frequencies of the Nyquist plots represents the charge transfer resistance (Rct) at the compound-electrolyte interface, and the straight line in the low frequency region shows that ionic diffusion appears during charging-discharging process. It is found that the Rct value of SMM (0.912 Ω) are lower than that of $MnO_2$ powders (1.213Ω), indicating a higher electron transport of SMM. In addition, the SMM-based electrode shows a much sharper slope, implying better ion diffusion properties.[24]

Long-term galvanostatic charge–discharge stability of the SMM-based electrode is also investigated, and the variation of the specific capacitance value during 1000 cycles is depicted in Fig. 3f. The specific capacitance value increases initially with the increase of the cycle number due to the encounter of electrochemical activation, which promotes the diffusion of electrolytes into the

oxide matrix, resulting in a decrease in the charge-transfer resistance of redox couples since electron transfer and proton exchange occur simultaneously during the redox transition.[25] The discharge specific capacitance still keeps about 105% after 1000 cycles, indicating that the SMM-based electrode has good long term electrochemical stability and the repetitive charge–discharges do not induce noticeable degradation of the microstructures. The excellent stability is probably due to the high mechanical strength of SMM deriving from its long and tangled nanotube structure as demonstrated in Fig. 2c.

## Conclusions

Based on the above discussions, we propose that the PU foam template holds great promise for the synthesis of monolithic nanomaterials. The as-prepared $MnO_2$ nanotube monolith with 3D interconnected foam structure, macroporous channels, and mesoporous tube structure shows superior capacitive properties as supercapacitor electrode materials. This remarkable performance can be attributed to the unique microstructure that facilitates the transport of ions and electrons and enhance the utilization of active materials. This simple and effective method should be viable to extend to other nanomaterial monoliths. Work in this direction is ongoing in our lab.

## Acknowledgements

This work was financially supported by National Natural Science Foundation of China (Grant no. 21403302) and the Fundamental Research Funds for the Central Universities (Grant no. 15CX08010A).

## Notes and references

1 M. E. Davis, *Nature*, 2002, **417**, 813.
2 Y. Wan, Y. Shi and D. Zhao, *Chem. Mater.*, 2008, **20**, 932.
3 C. S. Cundy and P. A. Cox, *Chem. Rev.*, 2003, **103**, 663.
4 J. Beck, J. Vartuli, W. Roth, M. Leonowicz, C. Kresge, K. Schmitt, C. Chu, D. Olson and E. Sheppard, *J. Am. Chem. Soc.*, 1992, **114**, 10834.
5 J. Rouquerol, D. Avnir, C. Fairbridge, D. Everett, J. Haynes, N. Pernicone, J. Ramsay, K. Sing and K. Unger, *Pure Appl. Chem.*, 1994, **66**, 1739.
6 F. Li, Z. Wang, N. S. Ergang, C. A. Fyfe and A. Stein, *Langmuir*, 2007, **23**, 3996.
7 F. Caruso, R. A. Caruso and H. Möhwald, *Chem. Mater.*, 1999, **11**, 3309.
8 H. Yan, C. F. Blanford, B. T. Holland, W. H. Smyrl and A. Stein, *Chem. Mater.*, 2000, **12**, 1134.
9 H. Wakayama and Y. Fukushima, *Chem. Mater.*, 2000, **12**, 756.
10 Z.-Y. Yuan and B.-L. Su, *J. Mater. Chem.*, 2006, **16**, 663.
11 N. J. Coville and A. M. Tshavhungwe, *S. Afr. J. Sci.*, 2010, **106**, 1.
12 S. H. Lee, H. W. Kim, J. O. Hwang, W. J. Lee, J. Kwon, C. W. Bielawski, R. S. Ruoff and S. O. Kim, *Angew. Chem. Int. Ed.*, 2010, **49**, 10084.
13 N. Brun, S. R. S. Prabaharan, C. Surcin, M. Morcrette, H. Deleuze, M. Birot, O. Babot, M.-F. Achard and R. Backov, *J. Phys. Chem. C*, 2012, **116**, 1408.
14 D. Kuang, T. Brezesinski and B. Smarsly, *J. Am. Chem. Soc.*, 2004, **126**, 10534.
15 W. Chen, R. Rakhi, L. Hu, X. Xie, Y. Cui and H. Alshareef, *Nano Lett.*, 2011, **11**, 5165.
16 Y. Huang, Y. Huang, W. Meng, M. Zhu, H. Xue, C. S. Lee and C. Zhi, *ACS Appl. Mater. Interfaces*, 2015, **7**, 2569.
17 Y. Huang, H. Hu, Y. Huang, M. Zhu, W. Meng, C. Liu, Z. Pei, C. Hao, Z. Wang and C. Zhi, *ACS nano*, 2015, 9, 4766.
18 H. B. Wu, H. Pang and X. W. D. Lou, *Energy Environ. Sci.*, 2013, **6**, 3619.
19 M. Kruk and M. Jaroniec, *Chem. Mater.*, 2001, **13**, 3169-3183.
20 S. Devaraj and N. Munichandraiah, *J. Phys. Chem. C*, 2008, **112**, 4406.
21 C. Yuan, L. Hou, L. Yang, D. Li, L. Shen, F. Zhang and X. Zhang, *J. Mater. Chem.*, 2011, **21**, 16035.
22 G. Zhu, L. Deng, J. Wang, L. Kang and Z.-H. Liu, *Colloids Surf. A: Physicochem. Eng. Aspects*, 2013, **434**, 42.
23 C. Yuan, H. B. Wu, Y. Xie and X. W. D. Lou, *Angew. Chem. Int. Ed.*, 2014, **53**, 1488.
24 Z. Yang, F. Xu, W. Zhang, Z. Mei, B. Pei and X. Zhu, *J. Power Sources*, 2014, **246**, 24.
25 Y.-T. Wu and C.-C. Hu, *J. Electrochem. Soc.*, 2004, **151**, A2060.